Electronic structure of the double-perovskite Ba$_2$FeMoO$_6$ using photoemission spectroscopy

J.-S. Kang,[1] H. Han,[2] B. W. Lee,[2] C. G. Olson,[3] S. W. Han,[4] K. H. Kim,[4] J. I. Jeong,[5] J. H. Park,[6] and B. I. Min[6]

[1]*Department of Physics, The Catholic University of Korea, Puchon 422-743, Korea*

[2]*Department of Physics, Hankuk University of Foreign Studies, Yongin, Kyungki 449-791, Korea*

[3]*Ames Laboratory, Iowa State University, Ames, Iowa 50011*

[4]*Department of Physics, Gyeongsang National University, Chinju 660-701, Korea*

[5]*Research Institute of Industrial Science and Technology, Pohang 790-600, Korea*

[6]*Department of Physics, Pohang University of Science and Technology, Pohang 790-784, Korea*

The electronic structure of Ba$_2$FeMoO$_6$ (BFMO) has been investigated by using photoemission spectroscopy (PES). By varying $h\nu$ across the Mo $4d$ Cooper minimum, it is found that the states close to the Fermi level E_F are predominantly of the Mo $t_{2g}\downarrow$ and Fe $t_{2g}\downarrow$ character. The measured PES spectrum is compared to the calculated electronic structure obtained in the local spin-density approximation (LSDA) and LSDA$+U$ methods. The LSDA$+U$ calculation yields better agreement with experiment in the peak positions than does the LSDA calculation. The present study supports the double exchange mechanism for the half-metallic ferrimagnetism in BFMO.

I. INTRODUCTION

Since the discovery of the colossal magnetoresistance (CMR) phenomenon in the doped perovskite Mn oxides $R_{1-x}A_x$MnO$_3$ (RAMO; R is a rare earth, and A a divalent cation),[1] even room-temperature magnetoresistance (MR) has been observed in ordered double perovskite oxides with very high magnetic transition temperatures T_C ($\simeq 330$–450 K): A_2FeMoO$_6$ ($A=$Ca,Sr,Ba).[2–4] Much of the current interest in double perovskites is focused on the high T_C and the low field MR, which suggest high spin polarization of conduction electrons and a half-metallic ground state.[2] The question arises whether the essential physics of A_2FeMoO$_6$ is similar to that of RAMO manganites. The metallic conductivity and ferromagnetism in doped RAMO systems have been explained by the double exchange (DE) mechanism[5] between spin-aligned Mn^{3+} ($t_{2g}^3 e_g^1$) and Mn^{4+} (t_{2g}^3) ions. Further, the strong electron-phonon interaction due to the Jahn-Teller effect at the Mn^{3+} ion is invoked to elucidate the metal-insulator (M-I) transition in RAMO's.[6–8] In the DE model, there should exist mixed-valent ions to maintain the correlation between magnetism and conductivity.

The lattice of A_2FeMoO$_6$ consists of alternating FeO$_6$ and MoO$_6$ octahedra. Magnetization data for Sr$_2$FeMoO$_6$ (SFMO) indicate ferrimagnetic coupling between Fe^{3+} ($3d^5; t_{2g}^3 e_g^2, S=5/2$) and Mo^{5+} ($4d^1; t_{2g}^1, S=1/2$) ions,[9] and the MR was interpreted as due to intergrain tunneling with the half-metallic electronic structure.[2,10–12] Neutron diffraction and Mössbauer spectroscopy on A_2FeMoO$_6$ indicated an Fe moment of (4.0–4.1)μ_B but negligible localized moment on Mo, about $-0.2\mu_B$.[3,13] The ferrimagnetic coupling between Fe^{3+} and Mo^{5+} can be understood in terms of superexchange through the Fe-O-Mo π bonding.[14,15] The high T_C suggests a large interatomic exchange coupling between Fe and Mo ions. The superexchange model, however, is not compatible with the metallic nature of Ba$_2$FeMoO$_6$ (BFMO).

Thus the origin of the high T_C ferrimagnetism and the low field MR in double perovskites remains to be determined.

Therefore it is essential to know the valence states of A and Fe ions in A_2FeMoO$_6$ to understand the underlying physics properly. In particular, the valence states of Fe and Mo ions and the half-metallic electronic structure of A_2FeMoO$_6$ have not been confirmed experimentally. Despite extensive photoemission spectroscopy (PES) studies on the manganites,[16–24] no PES study has been reported on A_2FeMoO$_6$-type double perovskites yet except for the Mo $3d$ core-level PES of SFMO.[25] In this paper, we report a photoemission spectroscopy study of Ba$_2$FeMoO$_6$. Experimental results are compared to the calculated electronic structure. Note that the reported room-temperature MR in BFMO is larger than that in SFMO, even though T_C of SFMO is much higher.[11]

II. EXPERIMENTAL AND CALCULATIONAL DETAILS

A polycrystalline BFMO sample was prepared by the standard solid-state reaction method. A stoichiometric mixture of high purity (99.99% or better) BaCO$_3$, Fe$_2$O$_3$, and MoO$_3$ powders was fired at 900 °C in air with several intermediate grindings, followed by a final grinding before the powder was pressed into pellets. The pellet was sintered in a stream of 5% H$_2$ in Ar at 1100 °C for 24 h. The x-ray diffraction peaks were indexed with respect to cubic symmetry ($Fm3m$). Superlattice lines such as (111) and (311) arising from the alternate ordering of Fe and Mo sites were observed in the x-ray diffraction pattern. Resistivity and magnetization measurements for BFMO showed very similar behaviors as in Refs. 3 and 11. The temperature dependent resistivity $\rho(T)$ exhibited a metallic behavior ($d\rho/dT>0$) in the ferrimagnetic state, with the residual resistivity of $\rho_0 \sim 0.002$ Ω cm at $T\lesssim 15$ K.

PES experiments were carried out at the Ames/Montana beamline at the Synchrotron Radiation Center (SRC). Samples were fractured and measured in vacuum with a base
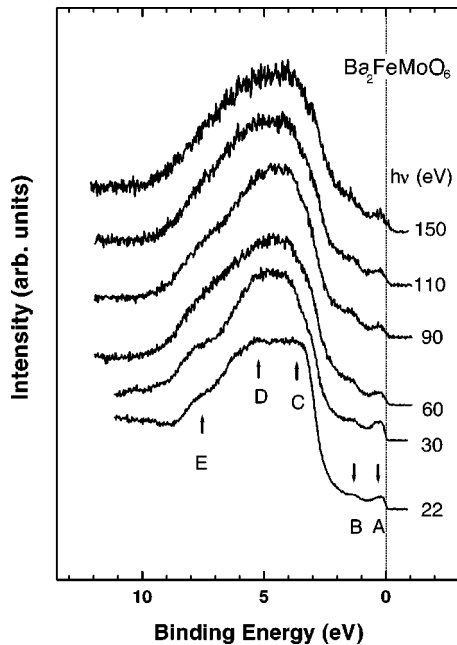
FIG. 1. Valence-band energy distribution curves of Ba_2FeMoO_6 (BFMO) over a photon energy ($h\nu$) range of $22\ eV \lesssim h\nu \lesssim 150\ eV$.
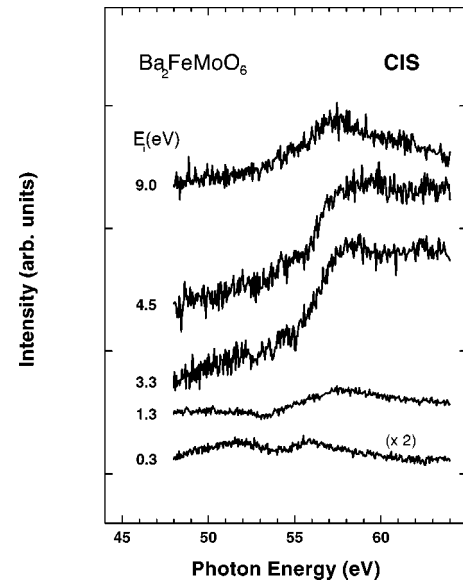

FIG. 2. Constant-initial-state (CIS) spectra of BFMO for several initial-state energies, taken across the Fe $3p \rightarrow 3d$ absorption threshold.

pressure better than 3×10^{-11} Torr and at $T \lesssim 15$ K. The Fermi level E_F of the system was determined from the valence band spectrum of a sputtered Pt foil. The total instrumental resolution (full width at half maximum) was about 100–250 meV at $h\nu = 20$–120 eV. All the spectra were normalized to the mesh current.

The electronic structure of BFMO was calculated by using a density-functional calculation within the local spin-density approximation (LSDA) and the LSDA+U (LSDA incorporating the on-site Coulomb interaction U) methods[26] on the basis of the linearized muffin-tin orbital band method. The von Barth–Hedin form of the exchange-correlation potential was utilized. The angular-momentum-projected local densities of states (PLDOS's) for BFMO were obtained for both LSDA and LSDA+U calculations by using 50 $\vec{k}$ points inside the irreducible Brillouin zone for integration.

III. RESULTS AND DISCUSSION

Figure 1 shows the valence-band spectra of BFMO for $22\ eV \lesssim h\nu \lesssim 150\ eV$. Each valence-band spectrum is scaled at the peak maximum, and presented on the binding energy (BE) scale. In principle, the different line shape with varying $h\nu$ reflects the matrix element effect, namely, the change in the relative strengths of the photoionization cross sections of the different electronic states with varying $h\nu$. In Fig. 1, however, the line shape of the valence-band spectrum of BFMO changes very little with varying $h\nu$. This is because the O $2p$ electron emission is dominant among the Fe $3d$, Mo $4d$, and O $2p$ valence electrons in BFMO for $22\ eV \lesssim h\nu \lesssim 150\ eV$. As $h\nu$ increases, the O $2p$ electron emission decreases slightly with respect to the other electron emissions. If one assumes $Fe^{3+}(3d^5)$, $Mo^{5+}(4d^1)$, and the

filled O $2p$ bands ($2p^6$) in BFMO, then the cross-section ratio of Fe $3d$:Mo $4d$:O $2p$ per unit cell of BFMO is about 4%:5%:91% at $h\nu \sim 20$ eV, and about 25%: $\sim 0\%$:75% at $h\nu \sim 90$ eV according to an atomic photoionization cross-section calculation.[27] A broad Cooper minimum[28] in the Mo $4d$ cross section occurs around $h\nu \sim 90$ eV, arising from the vanishing matrix elements for electron transitions to final states. Consequently the Mo $4d$ emission is negligible at $h\nu \sim 90$ eV.

A metallic Fermi edge is observed in the valence-band spectrum of BFMO obtained at $T \sim 15$ K, which confirms its metallic behavior at low T. The valence-band spectra of BFMO reveal several structures, labeled A (0.3 eV), B (1.3 eV), C (3.5 eV), D (5 eV), and E (8 eV). Even though the variation in the valence-band line shape is very weak, the intensity of the peak A (0.3 eV) relative to the peak B (1.3 eV) decreases as $h\nu$ increases from 30 eV to 90 eV. We interpret this behavior as due to the decreasing Mo $4d$ electron contribution to the peak A with increasing $h\nu$ toward the Mo $4d$ Cooper minimum. In fact, the peak A (0.3 eV) has strongly mixed electron character, i.e., it is predominantly of Mo $4d$ and Fe $3d$ electron character. This assignment will be further discussed in Figs. 2, 4, and 5 below. The peak B (1.3 eV) has Fe $3d$ electron character, strongly hybridized to the O $2p$ electrons. The relative intensities of the high BE peaks of C, D, and E (3.5–8 eV) remain nearly unchanged with changing $h\nu$, suggesting that they have predominantly O $2p$ electron character.

Figure 2 shows the constant-initial-state (CIS) spectra of BFMO for several initial-state binding energies E_i, taken in the Fe $3p \rightarrow 3d$ RPES (resonant PES) region. In this figure, the vertical scale is the same for all the curves. CIS spectra are obtained by varying $h\nu$ and E_K simultaneously so as to maintain $E_i = h\nu - \phi - E_K$ constant (ϕ is the work function, E_K the kinetic energy). Thus the CIS spectrum measures the
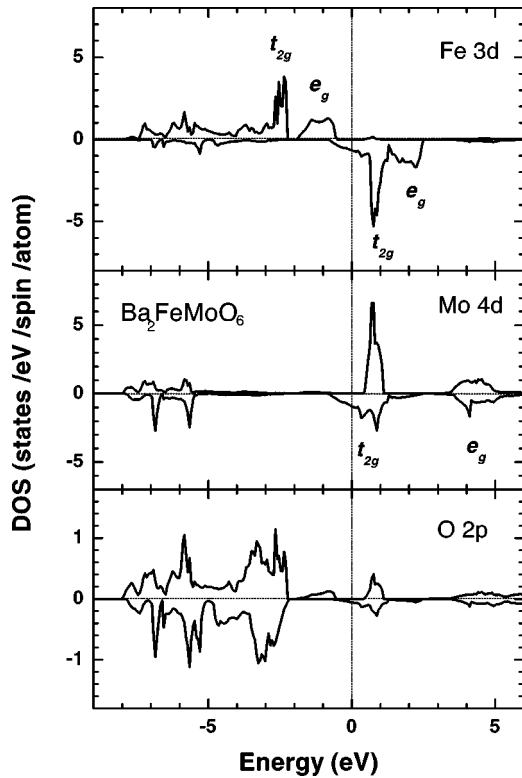
FIG. 3. The calculated projected local density of states (PLDOS) for BFMO, obtained under the LSDA. The top panel shows the majority-spin and minority-spin Fe $3d$ PLDOS's per atom. The lower two panels show the same for the Mo $4d$ and O $2p$ states, respectively.

relative strength of a given initial-state emission as a function of $h\nu$.[29] The resonant features observed in this figure are due to the Fe $3p \to 3d$ resonance.[30] The large features for $E_i = 3.3$ and 4.5 eV indicate that the Fe $3d$ electron character is concentrated predominantly under the main peak of the valence band, around 3–5 eV BE. Note, however, that there is also Fe $3d$ electron character around peak B (1.3 eV) and peak A (near E_F), even though their interference features are weak. This observation supports the finding of Fig. 1, and is also consistent with the LSDA calculation shown in Fig. 3.

To understand the microscopic origin of the valence-band electronic structure of BFMO, a LSDA electronic structure calculation has been performed for BFMO at the experimental lattice constant $a = 8.063$ Å.[3] The results are shown in Fig. 3. The upper and lower curves represent the majority-spin and minority-spin PLDOS's per atom, respectively. The calculated electronic structure of BFMO is qualitatively similar to that of SFMO, and shows half-metallic nature.[2,31] That is, the majority-spin electrons are insulating while the minority-spin electrons are metallic, resulting in 100% spin-polarized conduction electrons at E_F. As shown in this figure, the spins of the Fe and Mo ions are polarized antiferromagnetically. The similarity in the peak positions as well as in the intensity distribution of the Fe $3d$, Mo $4d$, and O $2p$ PLDOS's reflects the large hybridization between the Fe d and O p states and between the Mo d and O p states. The Fe $3d$ states show a large exchange splitting of ~ 4 eV, while
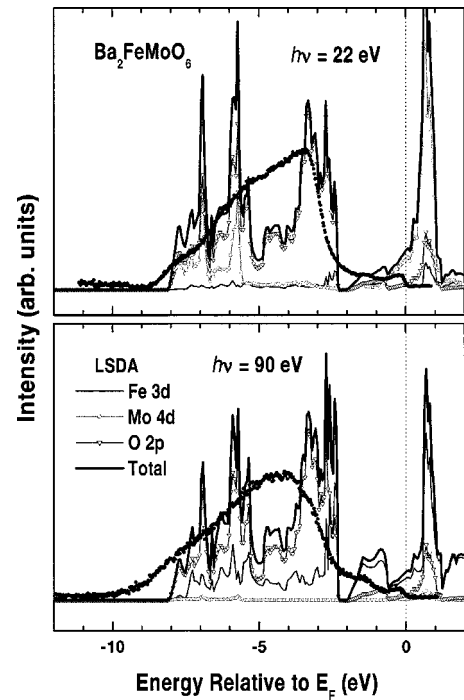

FIG. 4. Top: Comparison of the $h\nu = 22$ eV valence-band spectrum of BFMO (dots) to the weighted sum of the calculated PLDOS's (solid lines) obtained from the LSDA calculation. Bottom: The same for $h\nu = 90$ eV.

the Mo $4d$ and O $2p$ states show negligible exchange splitting. Most of the O $2p$ PLDOS is located between -2 eV and -8 eV, and its contribution near E_F is small, consistent with the very weak intensity near E_F in the PES spectrum at a low $h\nu$ (Fig. 1). The majority-spin Fe $3d$ bands are fully occupied, and the minority-spin Fe $t_{2g}\downarrow$ bands are occupied by about 0.5–1 electron, implying that the Fe valence is about $+2 - +2.5$. As to the Mo $4d$ bands, about one electron is occupied in the minority-spin $t_{2g}\downarrow$ bands, and so the nominal valence corresponds to Mo^{5+}. The charge neutrality in BFMO is satisfied because the O $2p$ bands are not completely occupied, as shown at the bottom of Fig. 3. The region near E_F (-1 eV $\lesssim E \lesssim E_F$) is contributed by the Mo $t_{2g}\downarrow$ and Fe $t_{2g}\downarrow$ states, which are hybridized with the O $2p$ states. The contribution from Mo $t_{2g}\downarrow$ is larger, 1.0 states/eV at E_F, as compared to 0.7 states/eV from Fe $t_{2g}\downarrow$.

Figure 4 compares the measured valence-band PES spectra to the theoretical spectra, obtained from the LSDA calculation. The theoretical spectra were obtained by adding the Fe d, Mo d, and O p PLDOS's per formula unit after they are multiplied by the corresponding photoionization cross sections.[27] The inelastic backgrounds have been subtracted from the valence-band spectra by assuming that the amount of the background is proportional to the total integrated intensity at higher E_K's. The experimental and theoretical curves are scaled to each other so that the area underneath each curve is roughly the same. As explained in Fig. 1, the O $2p$ emission is dominant in the $h\nu = 22$ eV spectrum. In the $h\nu = 90$ eV spectrum, the Mo $4d$ emission is suppressed due

to the Mo $4d$ Cooper minimum, and so the Fe $3d$ emission is visible ($\sim 25\%$ of the total emission).

This figure provides the following information. First, the $h\nu = 90$ eV spectrum still contains the pronounced features of the peaks A and B, as denoted in Fig. 1. Since most of the O $2p$ states are concentrated in the region -2 to -8 eV (Fig. 3) and the Mo $4d$ emission is suppressed at $h\nu = 90$ eV, this observation indicates that both A and B have substantial Fe $3d$ electron character. In particular, the finding that the states just below E_F have substantial Fe $3d$ electron character indicates that the Fe $t_{2g}\downarrow$ band should be partially occupied.[32] If the minority-spin Fe $t_{2g}\downarrow$ band is occupied by about one electron, then the electronic configuration of the Fe ion is $3d^{5+x}$ ($x \simeq 1$), i.e., $t_{2g}^3 \uparrow e_g^2 \uparrow t_{2g}^x \downarrow$, implying that the Fe valence is far from $+3$, but $3-x$. Secondly, the intensity of the peak B relative to the peak A at $h\nu = 90$ eV becomes higher than that at $h\nu = 22$ eV. As mentioned above, such a change is interpreted as due to the decreasing Mo $4d$ electron contribution to the peak A with increasing $h\nu$ toward the Cooper minimum, indicating that the peak A certainly has Mo $4d$ electron character. This finding is consistent with that in Fig. 3 that the Mo $4d$ ($t_{2g}\downarrow$) states below E_F are located between -1 eV and E_F.

To summarize, the states just below E_F have both Fe $3d$ and Mo $4d$ character, suggesting that it does not make sense to assign definite valences to Fe and Mo ions in BFMO. Since the Fe $t_{2g}\downarrow$ and Mo $t_{2g}\downarrow$ bands are almost degenerate, it is rather likely that two valence states Fe^{3+}-Mo^{5+} and Fe^{2+}-Mo^{6+} are degenerate and produce a type of DE interaction.[33] That is, hopping of itinerant $t_{2g}\downarrow$ electrons between Fe and Mo sites yields a kinetic energy gain so as to induce ferrimagnetism between Fe and Mo spins. This mechanism would explain both the half metallicity and the ferrimagnetism in BFMO. The difference from the case of CMR manganites is that the spins of itinerant carriers in BFMO are opposite to the localized Fe spins ($t_{2g}^3 \uparrow e_g^2 \uparrow$), satisfying the Hund rule.

Before moving to the issue of Coulomb correlation, it might be worthwhile to mention the magnetic mechanisms in double perovskites: superexchange versus DE interaction. Ferrimagnetism in the double perovskites $A_2 BB'O_6$ has been understood in terms of the superexchange interaction between B and B' d electrons through O p electrons. In general, the superexchange interaction works for localized systems, that is, for systems where d electrons of both B and B' atoms are localized. So ferrimagnetism in insulating double perovskites such as Sr_2MnMo_6, Sr_2CoMo_6, Ba_2MnMo_6, and Ba_2CoMo_6 can be explained based on the superexchange interaction. In these systems, the valencies of transition-metal atoms are expected to be integer. In contrast, SFMO and BFMO are different in the sense that these systems are not only ferrimagnetic but also metallic. The minority-spin t_{2g} bands of both Fe $3d$ and Mo $4d$ states are itinerant and degenerate near E_F (see Fig. 3), resulting in noninteger valencies of Fe and Mo ions. Indeed, recent Mössbauer experiments for SFMO indicate an intermediate valence state of Fe ions between Fe^{2+} and Fe^{3+}.[34,35] Therefore it is reasonable to think that magnetism in metallic
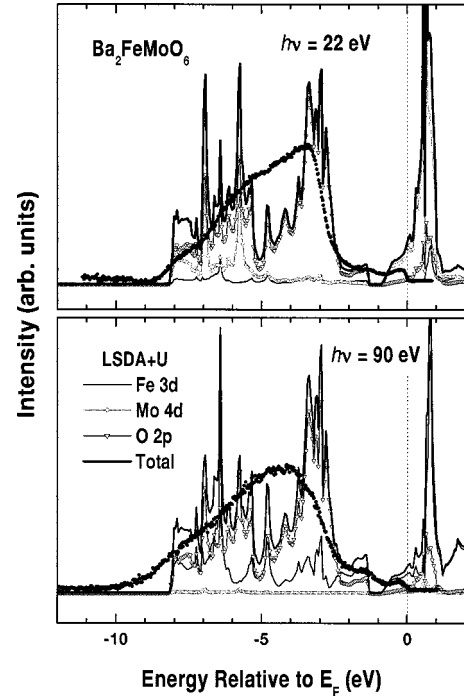

FIG. 5. Top: Comparison of the $h\nu = 22$ eV valence-band spectrum of BFMO (dots) to the weighted sum of the PLDOS's (solid lines) obtained from the LSDA+U calculation. Bottom: Similarly for $h\nu = 90$ eV.

SFMO and BFMO arises from hopping of itinerant t_{2g} electrons between Mo and Fe sites. This is a kind of DE interaction and is consistent with the calculated half-metallic electronic structure (see Fig. 3). In the DE mechanism, the magnetic transition temperature T_C is proportional to the hopping strength, i.e., the bandwidth of itinerant $t_{2g}\downarrow$ states.[36] Hence T_C can be high for SFMO and BFMO. The observed correlation between T_C and the estimated bandwidth in $AA'FeMoO_6$ ($AA' =$ BaBa, BaSr, SrSr, CaCa) provides evidence for the operation of the DE interaction in metallic double perovskites.[37]

The LSDA calculation shows that the calculated bandwidth is comparable to the measured valence-band width, but that the peak positions in the LSDA appear at lower BE's than in the PES spectra. In order to explore the origin of this disagreement between experiment and theory, the on-site Coulomb correlation parameter U for the Fe $3d$ electrons is incorporated in the electronic structure calculation for BFMO. The parameters used in this calculation are the Coulomb correlation $U = 3.0$ eV and the exchange $J = 0.97$ eV. As in the LSDA, the LSDA+U calculation also yields half-metallic electronic structure for BFMO. The calculated magnetic moments for Fe and Mo are $3.97\mu_B$ and $-0.41\mu_B$ for the LSDA and $4.03\mu_B$ and $-0.46\mu_B$ for the LSDA+U, respectively. Note that both methods yield integer total magnetic moments ($4.00\mu_B$) per formula unit, which is consistent with the half-metallic nature of BFMO.

Figure 5 compares the LSDA+U calculation to the valence-band spectra, similarly to Fig. 4. Indeed the on-site Coulomb interaction between the Fe $3d$ orbitals in the LSDA+U calculation induces a larger separation between

Fe majority- and minority-spin bands. In consequence, the peak positions below E_F shift toward higher BE by 0.5–1 eV, resulting in better agreement with experiment for the LSDA+U than for the LSDA. Note that the feature B (as denoted in Fig. 1), which has mainly Fe $3d$ electron character, exhibits better agreement with the LSDA+U (Fig. 5) than with the LSDA (Fig. 4). The assignments of the electronic states for the peaks A and B are similar to those made in Fig. 4. These findings suggest the importance of the Fe $3d$ on-site Coulomb interaction in determining the electronic structure of BFMO.

IV. CONCLUSIONS

We have performed valence-band PES measurements for BFMO, and calculated the electronic structure of BFMO using both the LSDA and LSDA+U methods. By varying $h\nu$ across the Mo $4d$ Cooper minimum, the different electronic character of the valence band has been identified. It is observed that the states close to E_F are predominantly of Mo $t_{2g}\downarrow$ and Fe $t_{2g}\downarrow$ character. This finding suggests that the configuration of the $3d$ electrons at the Fe ion is $t_{2g}^3\uparrow e_g^2\uparrow t_{2g}^x\downarrow$, corresponding to Fe^{3-x} ($x\simeq0.5$–1) but far from Fe^{3+}. Most of the O $2p$ states are concentrated between -2 eV and -8 eV, and its contribution at E_F is small. The calculated PLDOS's reveal large hybridization between the Fe d and O p states and between the Mo d and O p states. The LSDA calculation shows reasonably good agreement with experiment in the bandwidth, but not in the peak positions. The LSDA+U calculation yields better agreement with experiment in the peak positions, suggesting the importance of the large on-site Coulomb interaction between Fe electrons in the electronic structure of BFMO. This study suggests that a kind of DE interaction is operative to produce the half metallicity and ferrimagnetism in BFMO.

[1] S. Jin, T.H. Tiefel, M. McCormack, R.A. Fastnacht, R. Ramesh, and L.H. Chen, Science **264**, 413 (1994).

[2] K.-I. Kobayashi, T. Kimura, H. Sawada, K. Terakura, and Y. Tokura, Nature (London) **395**, 677 (1998).

[3] R.P. Borges, R.M. Thomas, C. Cullinan, J.M.D. Coey, R. Suryanarayanan, L. Ben-Dor, L. Pinsard-Gaudart, and A. Revcolevschi, J. Phys.: Condens. Matter **11**, L445 (1999).

[4] Y. Moritomo, Sh. Xu, A. Machida, T. Akimoto, E. Nishibori, M. Takata, and M. Sakata, Phys. Rev. B **61**, R7827 (2000).

[5] C. Zener, Phys. Rev. **82**, 403 (1951).

[6] H. Röder, J. Zang, and A.R. Bishop, Phys. Rev. Lett. **76**, 1356 (1996).

[7] A.J. Millis, B.I. Shraiman, and R. Müller, Phys. Rev. Lett. **77**, 175 (1996).

[8] J.D. Lee and B.I. Min, Phys. Rev. B **55**, 12 454 (1997).

[9] F.S. Galasso, F.C. Douglas, and R.J. Kasper, J. Chem. Phys. **44**, 1672 (1966).

[10] T.H. Kim, M. Uehara, S.-W. Lee, and S. Lee, Appl. Phys. Lett. **74**, 1737 (1999).

[11] A. Maignan, B. Raveau, C. Martin, and M. Hervieu, J. Solid State Chem. **144**, 224 (1999).

[12] Y. Tomioka, T. Okuda, Y. Okimoto, R. Kumai, K.-I. Kobayashi, and Y. Tokura, Phys. Rev. B **61**, 422 (2000).

[13] B. Garcia-Landa, C. Ritter, M.R. Ibarra, J. Blasco, P.A. Algrabel, R. Mahendiran, and J. Garcia, Solid State Commun. **110**, 435 (1999).

[14] J.B. Goodenough, Phys. Rev. **100**, 564 (1955).

[15] J. Kanamori, Phys. Chem. Solids **10**, 87 (1959).

[16] A. Chainani, M. Mathew, and D.D. Sarma, Phys. Rev. B **47**, 15 397 (1993); A. Chainani, H. Kumigashira, T. Takahashi, Y. Tomioka, H. Kuwahara, and Y. Tokura, *ibid.* **56**, R15 513 (1997).

[17] T. Saitoh, A.E. Bocquet, T. Mizokawa, H. Namatame, A. Fujimori, M. Abbate, Y. Takeda, and M. Takano, Phys. Rev. B **51**, 13 942 (1995).

[18] D.D. Sarma, N. Shanthi, S.R. Krishnakumar, T. Saitoh, T. Mizokawa, A. Sekiyama, K. Kobayashi, A. Fujimori, Y. Takeda, and M. Takano, Phys. Rev. B **53**, 6873 (1996).

[19] J.-H. Park, C.T. Chen, S.-W. Cheong, W. Bao, F. Meigs, V. Chakarian, and Y.U. Idzerda, Phys. Rev. Lett. **76**, 4215 (1996).

[20] J.-H. Park, E. Vescovo, H.-J. Kim, C. Kwon, R. Ramesh, and T. Venkatesan, Nature (London) **392**, 794 (1998).

[21] D.S. Dessau, T. Saitoh, C.-H. Park, Z.-X. Shen, P. Villella, N. Hamada, Y. Moritomo, and Y. Tokura, Phys. Rev. Lett. **81**, 192 (1998).

[22] A. Sekiyama, S. Suga, M. Fujikawa, S. Imada, T. Iwasaki, K. Matsuda, K.V. Kaznacheyev, A. Fujimori, H. Kuwahara, and Y. Tokura, Phys. Rev. B **59**, 15 528 (1999).

[23] J.-S. Kang, C.G. Olson, J.H. Jong, H.J. Lee, T.W. Noh, and B.I. Min, Phys. Rev. B **60**, 13 257 (1999).

[24] J.-S. Kang, Y.J. Kim, B.W. Lee, C.G. Olson, and B.I. Min, J. Phys.: Condens. Matter **13**, 3779 (2001).

[25] D.D. Sarma, P. Mahadevan, T. Saha-Dasgupta, S. Ray, and A. Kumar, Phys. Rev. Lett. **85**, 2549 (2000).

[26] V.I. Anisimov, F. Aryasetiawan, and A.I. Liechtenstein, J. Phys.: Condens. Matter **9**, 767 (1997).

[27] J.J. Yeh and I. Lindau, At. Data Nucl. Data Tables **32**, 1 (1985). The photoionization cross sections in actual solids are different from the atomic photoionization cross sections.

[28] J.W. Cooper, Phys. Rev. **128**, 681 (1962); G.M. Bancroft, W. Gudat, and D.E. Eastman, Phys. Rev. B **17**, 4499 (1978).

[29] J.-S. Kang, C.G. Olson, T.W. Noh, and B.I. Min, J. Electron Spectrosc. Relat. Phenom. **114-116**, 683 (2001).

[30] L.C. Davis, J. Appl. Phys. **59**, R25 (1986).

[31] Y. Moritomo, Sh. Xu, T. Akimoto, A. Machida, N. Hamada, K.

Ohoyoma, E. Nishibori, M. Takata, and M. Sakata, Phys. Rev. B **62**, 14 224 (2000).

[32] Stricter assignment requires a spin-polarized photoemission spectroscopy study.

[33] A.W. Sleight and J.F. Weiher, J. Phys. Chem. Solids **33**, 679 (1972).

[34] J. Linden, T. Yamamoto, M. Karppinen, and H. Yamauchi, Appl. Phys. Lett. **76**, 2925 (2000).

[35] O. Chmaissem, R. Kruk, B. Dabrowski, D.E. Brown, X. Xiong, S. Kolesnik, J.D. Jorgensen, and C.W. Kimball, Phys. Rev. B **62**, 14 197 (2000).

[36] A. Chattopadhyay and A.J. Millis, cond-mat/0006208 (unpublished).

[37] C. Ritter, M.R. Ibarra, L. Morellon, J. Blasco, J. Garcia, and J.M. De Teresa, J. Phys.: Condens. Matter **12**, 8295 (2000).